International Journal of Heat and Mass Transfer 140 (2019) 877–885

Contents lists available at ScienceDirect

International Journal of Heat and Mass Transfer

journal homepage: www.elsevier.com/locate/ijhmt

Improvement of thermal performance of novel heat exchanger with latent heat storage

Wenzhu Lin [a], Rui Huang [a], Xiaoming Fang [a,b], Zhengguo Zhang [a,b,*]

[a] Key Laboratory of Enhanced Heat Transfer and Energy Conservation, The Ministry of Education, School of Chemistry and Chemical Engineering, South China University of Technology, Guangzhou 510640, China

[b] Guangdong Engineering Technology Research Center of Efficient Heat Storage and Application, South China University of Technology, Guangzhou 510640, China

ARTICLE INFO

Article history:
Received 4 March 2019
Received in revised form 11 June 2019
Accepted 11 June 2019
Available online 20 June 2019

Keywords:
Latent heat storage
Heat exchanger
Paraffin
Optimization

ABSTRACT

In this paper, an optimization method is proposed to improve the performance of a novel heat exchanger with latent heat thermal energy storage. Paraffin/expanded graphite composites were used as phase change material filled in annular tube, maintained contact with the shell and tube flow channels simultaneously. The heat transfer and flow characteristics of this novel heat exchanger were investigated in a previous study, which indicated that further research was required to enhance thermal transfer rates. Therefore, in this work, the thermal property of the material and geometric parameters of the heat exchanger, including compression density, tube diameter, and fins and baffle configuration, were studied numerically to improve the thermal behavior of the system. It was found that a composite with density of 600 kg/m^3, a tube diameter of 19 mm, and an extended surface and baffle space of 100 mm, can be used for the final optimization result. The results show that, after optimization, the thermal conductivity of the phase change material can reach 5.16 W/m K and the latent thermal energy stored in system could be twice that previously obtained. The solidification rate can increase to a maximum of 50% while the shell side Nu/Pr$^{1/3}$ can reach 29.98. The improved heat exchanger shows better energy storage capacity and working power.

1. Introduction

Currently, thermal energy storage (TES) plays an important role in overcoming the lack of balance between energy supply and demand. TES can be divided into three technologies: sensible, latent, and thermochemical. Latent heat thermal energy storage (LHTES) based on a phase change material (PCM) is considered to be a promising technique, because it has high energy storage density and low-fluctuation operating temperature [1]. Owing to the superior performance of the LHTES unit, it is employed in many fields, such as industrial waste heat recovery [2], solar energy utilization [3], thermal management of electron device [4], and building energy conservation [5].

A heat exchanger based on latent heat storage is the key of the LHTES unit. A cylindrical shell-and-tube heat exchanger is commonly used for heat storage system owing to its robust structure, easy maintenance, and high heat transfer rate [6]. Cano et al. [7] studied four types of PCMs filled in the shell side of the heat exchanger and the influence of the heat transfer flow rate, and different operation modes (watertight and countercurrent PCM flow) were evaluated. It was found that the shell-side PCM countercurrent flow system showed the best energy transfer performance. Hosseini et al. [8] investigated the melting and solidification performance of paraffin RT50 in the shell side of a shell-and-tube heat exchanger and found that by increasing the inlet water temperature from 70 °C to 80 °C, the charging and discharging efficiency of the heat exchanger rose from 81.1% to 88.4% and 79.7% to 81.4%, respectively. Kibria et al. [9] experimentally and numerically studied the latent heat storage system with shell and tube arrangement, where the PCM was filled in the shell and water passed through the tube. It was found that the influence of inlet temperature of the fluid on the solidification and melting of the PCM is considerable, whereas that of the mass flow rate is negligible.

In spite of the great potential of the LHTES system, the low thermal conductivity of the PCM still limits its practical feasibility. To overcome this drawback, various heat transfer enhancement techniques have been proposed, including the improvement of the thermo-physical properties of the material [10], extended surface in the PCM side [11], and optimization of the geometry configura-

* Corresponding author at: Key Laboratory of Enhanced Heat Transfer and Energy Conservation, The Ministry of Education, School of Chemistry and Chemical Engineering, South China University of Technology, Guangzhou 510640, China.
E-mail address: cezhang@scut.edu.cn (Z. Zhang).

https://doi.org/10.1016/j.ijheatmasstransfer.2019.06.040
0017-9310/

Nomenclature

B	baffle spacing (mm)
c_p	heat capacity (kJ kg^{-1} K^{-1})
d_i, d_a, d_0	diameter (mm)
D	shell diameter (mm)
E	energy (MJ)
h	heat transfer coefficient (W m^{-2} K^{-1})
l_i, l_a, l_0	length of tube (mm)
m	mass flow rate (kg s^{-1})
Nu	Nusselt number
P	average power (kW)
Pr	Prandtl number
Re	Reynold number
t, S_n	tube pitch (mm)
T	temperature (K)
u	velocity (m s^{-1})
V	volume flow rate (m^3 s^{-1})

Greek symbols

ρ	density (kg m^{-3})
η	dynamic viscosity (Pa s)
λ	thermal conductivity (W m^{-1} K^{-1})
τ	time (s)

Subscripts

a	annular tube
i	inside tube
in	inlet
o	shell side
out	outside

tion of the heat exchanger [12]. Tao et al. [13] used the orthogonal method to investigate the effects of the thermophysical properties of the PCM on the energy storage performance of a shell-and-tube heat exchanger. The numerical model was performed and validated, and the selection criteria of PCM is presented. Mahdi et al. [14] employed a nanoparticle-metal foam combination as heat transfer enhancement additive. The results show that the compound method greatly improves the PCM solidification rate, but metal foam porosity and nanoparticle volume fraction should be properly selected to ensure better performance. Incorporating extended surfaces is also an effective method to enhance the thermal performance of an LHTES unit. Khan et al. [15] investigated a shell-and-tube heat exchanger with longitudinal fins while paraffin (RT44HC) was employed as thermal storage material. It was observed that the novel longitudinal fins can effectively increase the overall thermal conductivity and phase transition rate. Pizzolato et al. [16] developed a design approach using topology optimization and multi-phase computational fluid dynamics to study highly conducting fins in shell-and-tube LHTES units. It was shown that fins with specific design features can remarkably enhance the natural convection of the PCM. Pirasaci et al. [17] studied the design of a latent heat storage unit and found that the length of storage and tube diameter have significant impact on effectiveness. Seddegh et al. [18] investigated the effect of geometrical parameters on a cylindrical shell-and-tube heat exchanger. The results show that a system with shell to tube radius ratio of 5.4 has better performance.

In general, the shell-and-tube heat exchangers with latent heat storage investigated before only have a single flow channel, mostly with the PCM in the shell side and heat transfer fluid (HTF) in the tube side, which limits their practical feasibility in a system with multi working fluid. The LHTES unit with multi flow channels still need to be studied. In our previous paper [19], a kind of novel structure latent heat storage heat exchanger with multi flow channels was presented and studied, in which PCM was filled in the annular tubes, whereas the working fluid flowed in the shell and tube channels. This kind of novel LHTES heat exchanger can be applied on many systems, such as those of gas waste heat recovery, which need multi flow channels for the working fluid – gas and water. Moreover, it can be used in a heat pump system, combined with on-peak and off-peak electricity, storing energy in the PCM and water at night, and releasing it for residential usage, which can increase the energy storage density of the traditional heat pump. A paraffin/expanded graphite (EG) composite is chosen to fill in the annular tube, which possesses desirable properties such as high latent heat, good stability, and high thermal conductivity, and it is non-corrosive [20]. The thermal conductivity of the paraffin/EG composite is approximately 10 times higher than that of paraffin, which can significantly increase the working power of the system. The preliminary study [19] indicated that this novel latent heat storage heat exchanger has high energy storage density and working power. Nevertheless, it also revealed that the thermal resistance of the PCM was relatively high, and the improvement of its overall thermal conductivity still needs further investigation.

Therefore, in this study, the emphasis was placed on the optimization of the thermal property of the PCM composite and the geometry configuration. The influence of the PCM thermophysical properties, tubes diameter, and fins and baffle configuration were investigated numerically based on a validated simulation model. The heat transfer characteristics of the HTF and PCM were analyzed in the solidification process by the commercial software FLUENT. This investigation can provide guidance for the usage and improvement of this novel structure heat exchanger, which can be applied into energy storage systems with multi working fluids, such as waste heat recovery energy storage and heat pump energy storage.

2. Mathematical modeling

2.1. Physical model

The physical geometry of this novel heat exchanger is depicted in Fig. 1, all dimensions are in millimeters. This shell-and-tube heat exchanger consists of the inner tube and outer annular tube filled with the PCM. This novel structure overcomes the shortcoming of the single-flow channel heat exchanger, and the PCM can transfer heat with the working fluid in the shell and tube simultaneously. It can be applied to latent heat storage systems with different working flows or discontinuous heating fluid. Paraffin with phase changing temperature between 45 and 50 °C was chosen as the PCM. However, paraffin is limited by its low thermal conductivity (0.24 W/m K), which can be solved by absorbing the liquid paraffin into a porous and high thermal conductivity material, expanded graphite, to form a stable composite. The detailed preparation method of the paraffin/EG composite can be found in a previous investigation [21]. The paraffin is heated up to 80 °C to completely melt and the EG absorbs the liquid paraffin by capillary force. After the PCM has been fully absorbed into the EG, it was cooled to from a stable composite. The prepared material is pressed into the annular tube of the heat exchanger, and the thermo-physical properties of the composite are listed in Table 1. The latent heat, specific heat, and phase change temperature of the composite

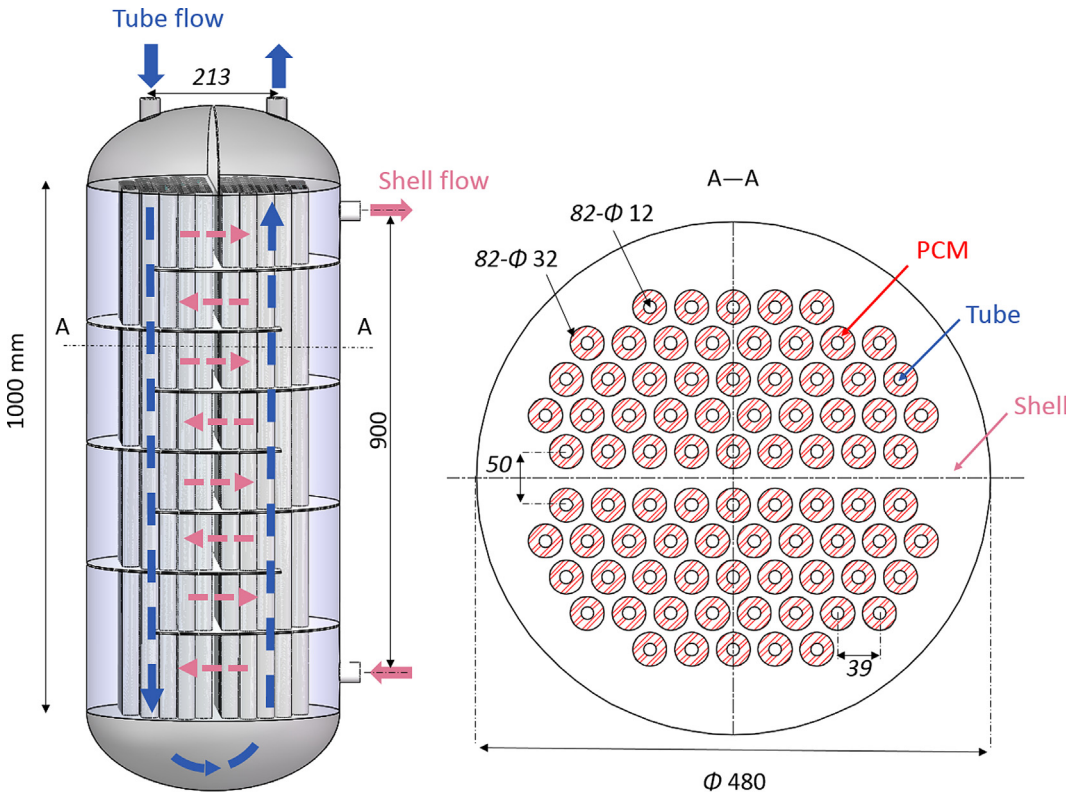

Fig. 1. The structure and streamline of novel LHTES heat exchanger.

material were measured by a differential scanning calorimeter (DSC, Q20, TA Instruments). The thermal conductivity was measured by the Hotdisk TPS 2500 thermal constants analyzer. The thermal conductivity of the composite is approximately 10 times higher than that of pure paraffin. Water is the working fluid, and it flows in the shell and tube during the charging or discharging process.

The geometric dimensions of the novel heat exchanger are provided in Table 2. The inside and annular tubes were arranged according to the equilateral triangle method. The annular tube length is L = 1000 mm, and the diameter of the inner and annular tubes are d_i = 12 mm and d_a = 32 mm, respectively. The segmental baffles were located in the shell side to support the tube bundle and maintain the transverse flow for shell side fluid.

The detailed flow characteristic and thermal performance of this novel heat exchanger were studied experimentally and numerically in our previous research [19]. Prior results showed that the overall heat transfer rate still needs to be further improved. Thus, in this study, the numerical method was adopted to optimize the heat transfer performance of the LHTES system. The properties of the PCM composite, tube diameter, extended surface, and arrangement of baffles were investigated in turn in this research.

Table 1
The thermo-physical properties of the paraffin/EG.

Property	Value
Density (kg/m^3)	300
Latent heat (J/g)	155
Melting temperature (°C)	50.87
Solidification temperature (°C)	44.93
Thermal conductivity (W/m K)	2.35
Specific heat (kJ/kg K)	1.7

Table 2
Geometry parameters of the latent heat exchanger.

Item	Dimensions and descriptions
Tube-side parameters	
d_i (mm)	12
Tube pitch t (mm)	39
Tube bundle pitch S_n (mm)	50
l_i (mm)	1000
Number of tubes	82
Inlet and outlet distance (mm)	213
Annular tubes parameters	
d_a (mm)	32
l_a (mm)	1000
Shell-side parameters	
d_o (mm)	480
l_o (mm)	1000
Inlet and outlet distance (mm)	900
Baffle parameters	
Baffle space B (mm)	115
Baffle height (mm)	360
Thickness (mm)	3
Material	Stainless steel

2.2. Grid generation and independence

The 3D geometry of the heat exchanger was built by the commercial software Solidworks, as Fig. 1 indicated. The mesh was generated by the pre-processing software packaged in ANSYS. Owing to the complicated structure of the shell side, the computational domain was meshed with tetrahedral grids, while the hexahedral mesh was chosen for the inside and annular tubes, as shown in Fig. 2. The independence of the grid number was carefully verified to obtain a numerical result with sufficient accuracy. Taking the shell-side outlet temperature and heat transfer rate as the

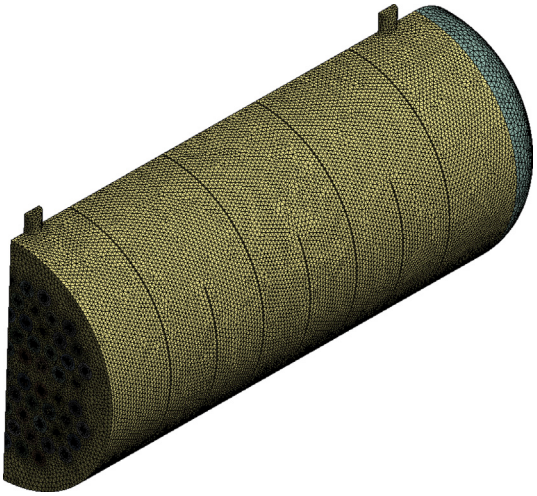

Fig. 2. Meshes of geometry model.

criterion, the deviation between models with 1.12×10^7 and 1.50×10^7 cells were less than 0.5 K and 1.0%. To achieve solution accuracy while still saving the calculation resource, the final model with 1.12×10^7 cells was adopted. The maximum skewness for the final mesh model was 0.80, which means that the mesh has relatively good quality for further calculation [19].

2.3. Numerical method and boundary condition

The enthalpy-based method assembled in the commercial software FLUENT is a common method to simulate solid and liquid phase changing performances of the material. In this study, the solidification and melting packing on FLUENT was used to evaluate the heat transfer performance of the heat exchanger with PCM. The standard k–ε model was adopted for the flow in the shell side while the laminar model applied to the tube-side flow regime.

To simplify the calculation and save resources, the following assumptions were made: (1) the physical thermal property of the material remains constant in the phase change period; (2) the natural convection and heat dissipated through radiation were neglected; (3) the outside wall of the heat exchanger was adiabatic. The SIMPLE algorithm scheme was adopted for the pressure-based solver used for spatial discretization. The convergence criterion for energy and continuity was of less than 10^{-7} and 10^{-4}, respectively. A parallel computer with 24 processes was run on a workstation with 32 Intel Xeon-core CPUs and 32 GB RAM. Approximately, 18 h to calculate a case.

The velocity inlet and pressure outlet were defined for the boundary condition in the simulation. Only the discharging process of the LHTES system was investigated in this study. The volume flow rate of water was set to be 1.2 m^3/h while the discharging temperature was 30 °C, and the initial temperate of whole system was 55 °C.

2.4. Model validation

The simulation result was compared to experimental data to validate the accuracy of the numerical model. The validation results can be referred to our previous research [19]. The numerical result shows good agreement with the experimental data. Outlet temperature for cooling process in shell side has the maximum absolute errors of 3.32 °C and average values of 0.75 °C. For charging process, the maximum and average value are 1.37 °C and 0.32 °C. The error can be explained by the unavoidable measurement uncertainty in the experiment, but also by the simplification of the computational model, boundary condition, and initial conditions, which can lead to the relative error. Therefore, it can be concluded that the numerical model is sufficiently accurate to investigate the heat transfer performance of this heat exchanger with LHTES.

3. Data reduction

To characterize and compare the heat transfer performance of the LHTES system, the following figures were calculated.

— Total energy; the following integral method is applied to calculate the total recovered energy from the LHTES system [22]:

$$E = \int_0^{\tau} \dot{m} c_p (T_{out} - T_{in}) \cdot d\tau \tag{1}$$

— Average power, calculated as recovered energy to duration time in the cooling process, as in the following equation:

$$P = \frac{\int_0^{\tau} \dot{m} c_p (T_{out} - T_{in}) \cdot d\tau}{\tau} \tag{2}$$

where $\dot{m}$ is the mass flow rate, c_p is the specific heat capacity, and T_{in} and T_{out} are the inlet and outlet temperatures of the HTF, respectively.

— Tube side heat transfer coefficient: the tube side heat transfer coefficient can be calculated by the Sieder-Tate equation [23] when Graetz (Gz) number is higher than 100 [24]. In our test, Gz number is in the range of 105 to 117.

$$Gz = Re \,\mathrm{Pr} \frac{d_i}{l} \tag{3}$$

$$h_i = \frac{Nu_i \lambda_i}{d_i} \tag{4}$$

where the Nusselt number and Reynold number can be calculated as follows:

$$Nu_i = 1.86 (Re_i \,\mathrm{Pr}_i)^{\frac{1}{3}} \left(\frac{d_i}{l}\right)^{\frac{1}{3}} \left(\frac{\eta}{\eta_w}\right)^{0.14} \tag{5}$$

$$Re_i = \frac{d_i u_i \rho}{\eta} \tag{6}$$

$$\mathrm{Pr} = \frac{\mu C_p}{\lambda} \tag{7}$$

— Shell side heat transfer coefficient: the shell side heat transfer coefficient with segmental baffles can be calculated by the Kern equation [25]:

$$Nu_0 = 0.36 Re_0^{0.55} \mathrm{Pr}_0^{1/3} (\eta/\eta_w)^{0.14} \tag{8}$$

$$h_0 = \frac{Nu_0 \lambda}{d_e}$$

where λ is the thermal conductivity of working fluid, d_e is the equivalent diameter calculated from Eq. (9) [26]:

$$d_e = \frac{4\left(\frac{\sqrt{3}}{2} t^2 - \frac{\pi}{4} d_i^2\right)}{\pi d_i} \tag{9}$$

u_0 is the velocity of HTF which can be calculated as the following equation:

$$u_0 = \frac{V_0}{S_0} \tag{10}$$

The flowing area can be calculated as follows [27]:

$$S_0 = BD\left(1 - \frac{d_i}{t}\right) \tag{11}$$

4. Results and discussion

4.1. Effect of thermal property of paraffin/EG

The low thermal conductivity of paraffin (0.24 W/m K) limits its application to energy storage systems. By absorbing the liquid paraffin into a porous structure of expanded graphite, it can significantly increase its thermal conductivity. In our previous investigation, paraffin with a 15% mass ratio of EG exhibited 2.35 W/m K of thermal conductivity (with 300 kg/m^3 density), which is approximately 10 times higher than that of pure paraffin. Based on the result of the investigation [19], the paraffin/EG's thermal conductivity was still not sufficient, and a large thermal resistance was caused when the HTF flow rate was high. Thus, the improvement of the thermal conductivity of the composite is necessary.

As EG is a porous matrix, the paraffin/EG composite has good compressibility. A higher compacted density of the paraffin/EG composite would significantly enhance its thermal conductivity [28]. A parametric investigation on different compression densities of the material is conducted, and five different densities are considered: 300, 400, 500, 600, and 700 kg/m^3. Based on the model of thermal conductivity of the organic PCM/EG proposed by Ling et al. [29], the specific thermal conductivity of the material at different densities can be obtained with a constant 85% mass ratio of PCM, as presented in Table 3. Based on the previous validated simulation model, the thermal performance of the system in the discharging process at different PCM's densities is numerically investigated. The HTF's flow rate is 1.2 m^3/h and the inlet temperature is 30 °C.

Fig. 3 depicts the pure paraffin and its EG composite's liquid fraction under the same working condition. It clearly shows that paraffin/EG can significantly increase the phase change rate of the material; paraffin/EG required approximately 600 s to completely solidify, while in 1000 s, the pure paraffin still had a liquid fraction of approximately 0.2, which means that part of the material had not yet released its latent heat completely. Therefore, paraffin/EG can remarkably improve the thermal performance of the system.

The outlet temperature of water in the shell side discharge simulation is depicted in Fig. 4. The PCM is initially at 55 °C in all cases. As the discharging process continues, the PCM starts to solidify and releases latent heat energy to the HTF. Three states can be clearly observed during the discharging process. The first one is liquid sensible cooling, in which the temperature decreases rapidly. Then, the PCM reaches the solidification temperature when it starts to release latent heat, and the curve starts to change slowly. The solid sensible-energy releasing region starts at the point when the PCM releases latent heat thoroughly and turns to a pure solid phase. Fig. 4 indicates that a system with higher PCM compression density has longer heat releasing duration time. A higher compression density provides greater weight of the PCM under the same volume, and therefore, a larger amount of energy transfer from PCM to HTF, which results in longer discharging time.

The energy gained by water and the average power in the discharging process of an LHTES system can be calculated from Eqs. (1) and (2). The data presented in Fig. 5 imply that by increasing the density (thermal conductivity) of PCM, the energy and power also rise. The release of energy is in the range of 15.2–19.6 MJ, whereas the outlet power is 16.9–21.8 kW. The system has high working power. The increase in energy is due to the larger amount of PCM with higher density under the same volume, while higher

Table 3
Thermal conductivity of different density of paraffin/EG.

Density (kg/m^3)	Thermal conductivity (W/m K)
300	2.35
400	3.44
500	4.30
600	5.16
700	6.02

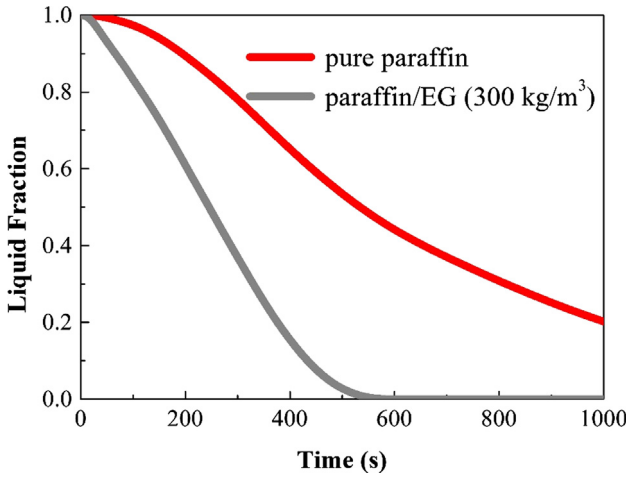

Fig. 3. Liquid fraction of paraffin and paraffin/EG composite.

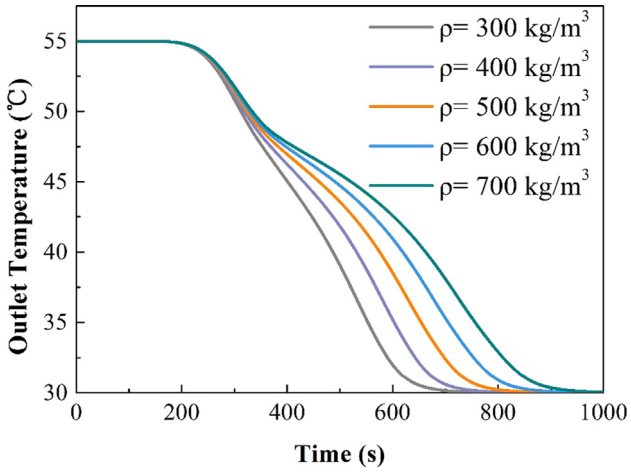

Fig. 4. Outlet HTF temperature curves in different PCM's density.

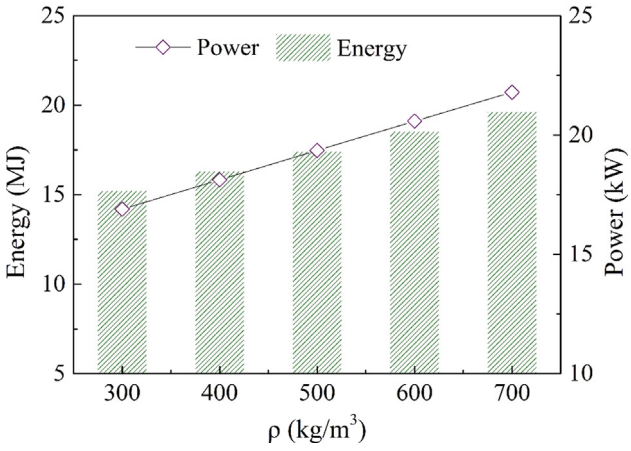

Fig. 5. Total energy and average power in different compression density.

thermal conductivity would result in a higher heat transfer rate between the PCM and HTF, which corresponds to a higher working power.

To observe the solidification process more intuitively, the temperature distributions inside the PCM container and the HTF when the working time is 400 s is illustrated in Fig. 6. The left and right parts of the contour represent the temperature of the HTF and PCM, respectively. It is clearly seen that both the PCM and water temperature gradually change along with the segmental baffle in the shell, which the same as the streamline of the working fluid shown in Fig. 1. From the above numerical results, higher density (higher thermal conductivity) of the composite will generate higher energy and power in the LHTES system. However, a highly compacted EG composite has unstable structure, and it presents a high volume expansion after the heating and cooling cycle [30]. Therefore, considering the overall performance, the material with density of 600 kg/m^3 and thermal conductivity 5.16 W/m K is selected.

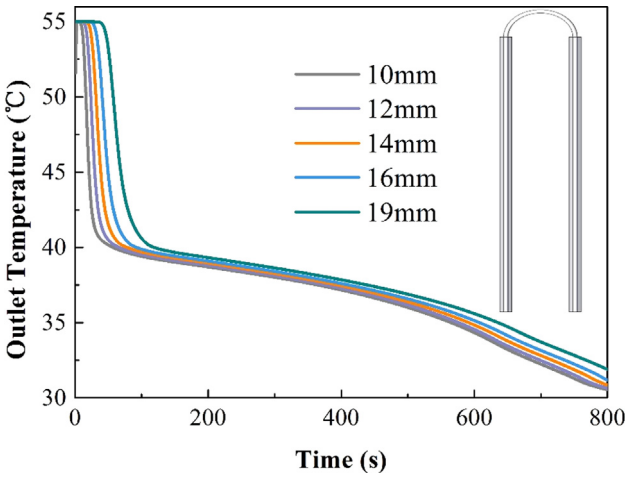

Fig. 7. Outlet temperature curves in different tube diameter.

4.2. Effect of diameter of inner tube

The tube diameter is further investigated to improve the heat transfer rate between the HTF and PCM. With the volume of PCM constant and density of 600 kg/m^3, the diameter of the inner tube is changed from 10 to 19 mm. To simplify the simulation, a single U-tube with annular PCM is used to study the solidification process of the system with different tube diameters. Water flows in the inner tube with 1.2 m^3/h flow rate and 30 °C inlet temperature. The outlet temperature of the HTF is shown in Fig. 7, and the energy gained by water and the average power are presented in Fig. 8. The outlet temperature of the HTF is always higher in the larger diameter tube, which corresponds to increasing released energy and working power. The energy ranges from 7.5 to 10.8 MJ while the power ranges from 9.8 to 12.0 kW, showing an increasing tendency with larger tube diameter. Under the same volume of PCM, the larger diameter tube indicates the thinner PCM annulus, which reduces the heat transfer distance from PCM to water. This will bring higher working power of system.

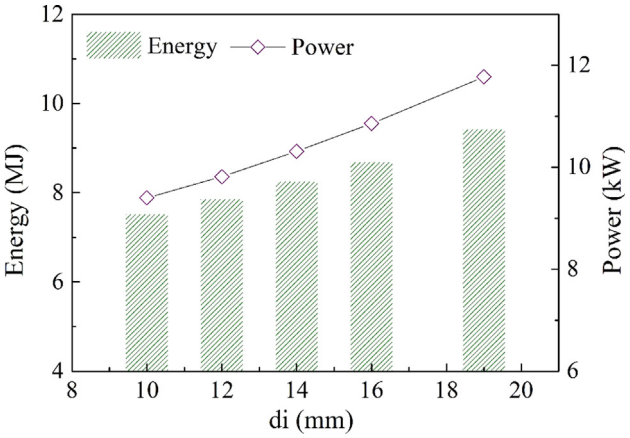

Fig. 8. Released energy and average power in different tube diameter.

From Eqs. (4)–(7), under the same mass flow rate of the HTF, the Reynolds number and heat transfer coefficient of the HTF in the tube reduce with higher tube diameter, as Fig. 9 illustrates. When the inner tube diameter changes from 10 to 19 mm, the Reynolds number changes from 1575 to 829, the tube side heat transfer coefficient changes from 494.8 to 230.7 W/(m^2 K), and both have decreasing trend. However, although the heat transfer coefficient decreases, the system's average working power increases with tube diameter, which can be explained by the increasing contact

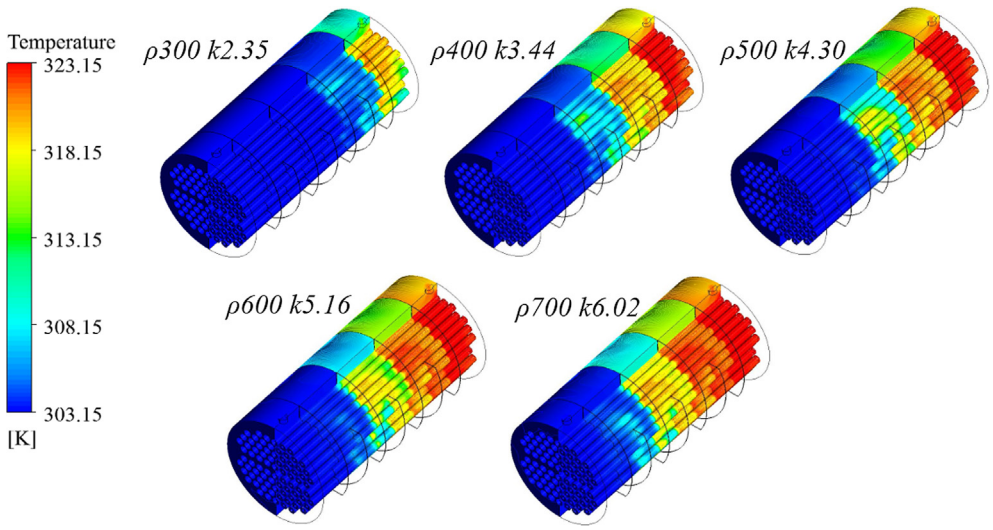

Fig. 6. Temperature contours of PCM and HTF in shell (Time = 400 s, V = 1.2 m^3/h).

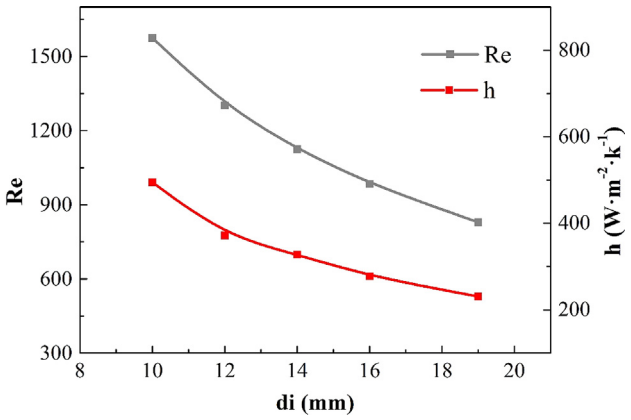

Fig. 9. Tube side Reynold number and heat transfer coefficient in different tube diameter. (V = 1.2 m^3/h).

surface between the PCM and HTF. It indicates that the increasing contact surface of the PCM has greater impact on the heat transfer process than the decreasing heat transfer coefficient. Even after the thermal conductivity reached 5.16 W/m K, the PCM still had a relatively high thermal resistance. Therefore, the extended surface has been further considered to increase the heat conductivity of the PCM with a constant tube diameter of 19 mm.

4.3. Effect of extended surface

To increase the thermal conductivity of the PCM further, seven fin geometries were developed, as tabulated in Table 4. Different numbers, shapes, and heights of fins were studied. Cases 1–4 investigated longitudinal fins with different heights, from 4 to 7 mm; cases 3 and 5 investigated different fin shapes, longitudinal and triangular; cases 1 and 6 and cases 3 and 7 studied different thicknesses of fins under the same volume. For simplicity, a single U-tube with annular PCM was applied to numerically investigate the PCM solidification process, with constant HTF flow rate of 1.2 m^3/h and temperature of 30 °C. The transient evolution of the liquid fraction of the PCM for cases 1–7 in the discharging process is plotted in Fig. 10.

Table 4
Different configurations of fins.

Case	Shape	Number	Height (mm)	Thickness (mm)
1	Longitudinal	8	4	0.2
2	Longitudinal	8	5	0.2
3	Longitudinal	8	6	0.2
4	Longitudinal	8	7	0.2
5	Triangular	8	6	0.4
6	Longitudinal	16	4	0.1
7	Longitudinal	16	6	0.1

As can be clearly observed, the liquid fraction of the PCM is 1.0 in the initial state for all cases, corresponding to the pure liquid phase. Then, with the release of energy, the PCM gradually turns into a solid phase and liquid fraction decrease. Fig. 10(a) indicates that in cases 1 to 4, the solidification rate of the PCM increases with higher fins, which can be easily explained by the increasing extended surface. However, when the height reaches 7 mm, the liquid fraction variation is almost the same as that with 6 mm. Therefore, longitudinal fins with 6 mm in height were chosen to investigate the different fin shapes further, under the same volume, as cases 3 and 5 indicate. A significant enhancement can be observed for the PCM solidification time using the PCM-longitudinal fin configuration, as shown in Fig. 10(b). It can be explained by the larger contact area of longitudinal fins. Cases 1 and 3 and cases 6 and 7 investigate different thicknesses of fins under a fixed volume. Fig. 10(c) clearly shows that case 6, with 16 fins and 0.1 mm in thickness, can enhance the thermal conductivity more than case 1. When the height reaches 6 mm (case 3), the solidification rate has small difference with that in case 7. Contact area in case 7 is significantly larger than case 3, but the heat transfer rate is unchanged, which means the thermal resistance has been eliminated. Therefore, the configuration in case 3 with 8 longitudinal fins and 6 mm in height is sufficient to optimize the thermal conductivity of the PCM composite (5.16 W/m K). The solidification rate of the PCM with extended surface can increase up to 50% compared with that obtained before.

The temperature contours in the same part of the transverse cross section, for similar conditions of the PCM-fins, are illustrated in Fig. 11. Comparing case 1 to cases 2 and 3, it is found that the height of the fin can significantly enhance the heat transfer rate of the system, and a complete solidification region (represented by the light green color) extended progressively. However, the

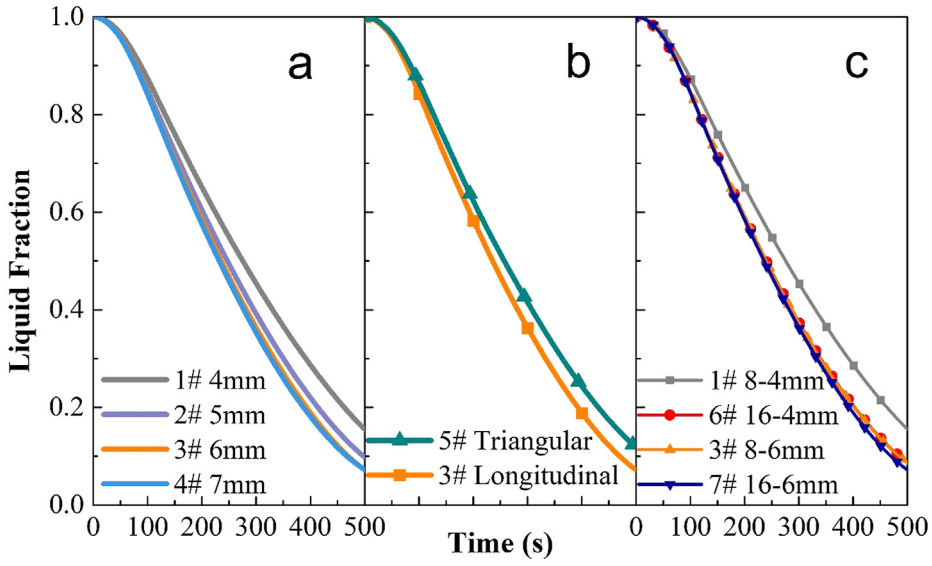

Fig. 10. Liquid fraction of PCM in different fin configurations. (a) Different height; (b) different shape; (c) different number.

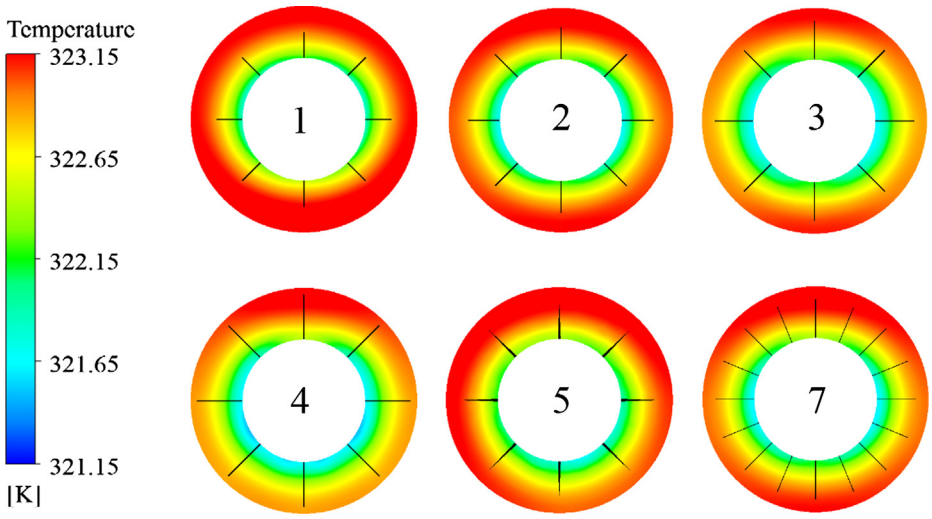

Fig. 11. Temperature contours of PCM in different fin configurations (Time = 200 s, z = 500 mm).

Table 5
Different parameters of baffle configuration.

Case	Number	Thickness (mm)	Baffle space (mm)	Cut ratio
1	7	3	125	25%
2	7	3	120	25%
3	8	3	112	25%
4	9	3	100	25%

temperature distribution in case 4, which has little difference with that in case 3, agrees well with the result in Fig. 10(a), in which the PCM solidification rate changes little with longitudinal fins of 6 and 7 mm in height. Under the same height, the longitudinal fins (case 3) show better performance in heat transfer rate enhancement than the triangular ones (case 5), and this also fits with what was indicated in Fig. 10(b). Considering the heat transfer performance and production cost, the final configuration in case 3 with 8 longitudinal fins with 6 mm height and 2 mm thickness is chosen to improve the thermal conductivity of the PCM.

4.4. Effect of baffle configuration

Segmental baffles are commonly used in conventional shell and tube heat exchangers to support the tube bundle and improve the heat transfer rate. The use of segmental baffles changes the fluid flow in a zigzag manner across the tube bundle in the shell side and improves the heat transfer rate by enhancing the turbulence of the HTF. The segmental baffle previously studied [19] is considered to optimize the shell side heat transfer performance further. As Table 5 presents, four groups of segmental baffles with different spaces were designed and studied. Based on the constant length of the heat exchanger, the baffle space changes from 100 to 125 mm, while the number of baffles changes from 7 to 9. The discharging performance was investigated under the same working condition, and $Nu/Pr^{1/3}$ was taken as the criterion to evaluate the performance of the HTF [31], which can be calculated from Eq. (8). In addition, to investigate the comprehensive performance, the shell side heat transfer coefficient per unit pressure drop is adopted, which can be calculated from Eqs. (8)–(11), and the pressure drop can be obtained directly from the simulation data.

The correlations between Nu and Re for different spaces are obtained in Fig. 12. The value of $Nu/Pr^{1/3}$ decreases with the increasing space, corresponding to a relatively higher heat transfer rate in a smaller baffle space. However, the smaller baffle space will cause a higher fluid pressure drop; hence, the heat transfer coefficient per pressure drop was considered, as presented in the red curve in Fig. 12. The curve reduces first and then increases, showing a maximum value of 12.1 $W/(m^2\ K\ Pa)$ in spaces of 100 and 125 mm. As the pressure drop is relatively low in the LHTES unit, this investigation mainly focuses on the improved heat transfer rate. Thus, the segmental baffle with 100 mm of space (case 4) is suitable for the shell side optimized parameter.

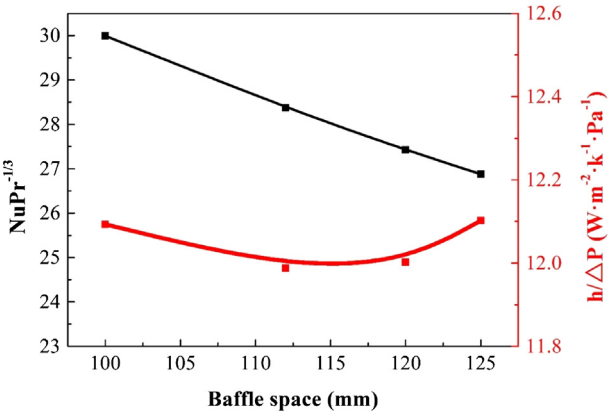

Fig. 12. Shell side $Nu/Pr^{1/3}$ and heat transfer coefficient per pressure drop versus baffle space.

5. Conclusions

In a previous study [19], we investigated a novel heat-exchanger structure having latent heat storage with multi flow channels. This novel structure can fix the shortcomings of the conventional heat exchanger in an LHTES system with single flowing channel, and it can be used in latent heat storage applications with different working flows or discontinuous heating sources. Based on the previous investigation result, the heat transfer rate of this novel heat exchanger still needs to be improved further. In this study, the PCM composite compression density (thermal conductivity), tube diameter, and fins and baffle configuration were investigated numerically to improve the heat transfer rate of the LHTES unit. The discharging process with constant flow rate of 1.2 m^3/h

and inlet temperature of 30 °C was studied based on the validated simulation model. The results are as follows:

1. The expanded graphite can significantly increase the thermal conductivity of the material and improve the working power of the system. Higher compression density of the composite led to higher heat storage capacity and thermal conductivity. The final paraffin/EG composite with density of 600 kg/m^3 and thermal conductivity of 5.16 W/m K was selected as the material. The shell side recovered energy was 18.52 MJ and the average power was 20.58 kW.
2. When the inner tube diameter changed from 11 to 19 mm with fixed PCM volume, although the Reynolds number and heat transfer coefficient of the HTF decreased with increasing tube diameter, the average working power increased. It can be explained by the larger contact heat transfer area of the PCM, which indicates that the PCM still has a relatively high thermal resistance in this system.
3. Different fin configurations were discussed to improve the heat transfer rate of the PCM further, and seven groups of fins were designed to investigate the effect of the shape, height, and thickness of the fin. The final longitudinal shape fin, with 6 mm in height, was able to eliminate the thermal resistance on the PCM.
4. Finally, the space of the segmental baffle in the shell was studied, showing a maximum heat transfer coefficient per pressure drop of 12.1 W/(m^2 K Pa) in spaces of 100 and 125 mm. Considering the overall performance, the final baffle with 100 mm was settled in the shell to achieve a better heat transfer rate, with $Nu/Pr^{1/3}$ of 29.98.

Declaration of Competing Interest

The authors declared that there is no conflict of interest.

Acknowledgments

This work was supported by the National Natural Science Foundation of China (No. U1507201), Guangdong Natural Science Foundation (2014A030312009) and the Applied Science and Technology Project of Guangdong Province (No. 2016B020243008).

References

[1] L. Fan, J.M. Khodadadi, Thermal conductivity enhancement of phase change materials for thermal energy storage: a review, Renew. Sustain. Energy Rev. 15 (1) (2011) 24–46.
[2] L. Miro, J. Gasia, L.F. Cabeza, Thermal energy storage (TES) for industrial waste heat (IWH) recovery: a review, Appl. Energy 179 (2016) 284–301.
[3] J. Pereira da Cunha, P. Eames, Thermal energy storage for low and medium temperature applications using phase change materials – a review, Appl. Energy 177 (2016) 227–238.
[4] Z. Ling, Z. Zhang, G. Shi, X. Fang, L. Wang, X. Gao, et al., Review on thermal management systems using phase change materials for electronic components, Li-ion batteries and photovoltaic modules, Renew. Sustain. Energy Rev. 31 (2014) 427–438.
[5] F. Souayfane, F. Fardoun, P.-H. Biwole, Phase change materials (PCM) for cooling applications in buildings: a review, Energy Build. 129 (2016) 396–431.
[6] Q. Wang, G. Chen, Q. Chen, M. Zeng, Review of improvements on shell-and-tube heat exchangers with helical baffles, Heat Transfer Eng. 31 (10) (2010) 836–853.
[7] D. Cano, C. Funez, L. Rodriguez, J.L. Valverde, L. Sanchez-Silva, Experimental investigation of a thermal storage system using phase change materials, Appl. Therm. Eng. 107 (2016) 264–270.
[8] M.J. Hosseini, M. Rahimi, R. Bahrampoury, Experimental and computational evolution of a shell and tube heat exchanger as a PCM thermal storage system, Int. Commun. Heat Mass Transfer 50 (2014) 128–136.
[9] M.A. Kibria, M.R. Anisur, M.H. Mahfuz, R. Saidur, I.H.S.C. Metselaar, Numerical and experimental investigation of heat transfer in a shell and tube thermal energy storage system, Int. Commun. Heat Mass Transfer 53 (2014) 71–78.
[10] C. Wang, T. Lin, N. Li, H. Zheng, Heat transfer enhancement of phase change composite material: copper foam/paraffin, Renew Energy 96 (2016) 960–965.
[11] M. Parsazadeh, X. Duan, Numerical study on the effects of fins and nanoparticles in a shell and tube phase change thermal energy storage unit, Appl. Energy 216 (2018) 142–156.
[12] R. Raud, M.E. Cholette, S. Riahi, F. Bruno, W. Saman, G. Will, et al., Design optimization method for tube and fin latent heat thermal energy storage systems, Energy 134 (2017) 585–594.
[13] Y.B. Tao, V.P. Carey, Effects of PCM thermophysical properties on thermal storage performance of a shell-and-tube latent heat storage unit, Appl. Energy 179 (2016) 203–210.
[14] J.M. Mahdi, E.C. Nsofor, Solidification enhancement in a triplex-tube latent heat energy storage system using nanoparticles-metal foam combination, Energy 126 (2017) 501–512.
[15] Z. Khan, Z.A. Khan, Experimental investigations of charging/melting cycles of paraffin in a novel shell and tube with longitudinal fins based heat storage design solution for domestic and industrial applications, Appl. Energy 206 (2017) 1158–1168.
[16] A. Pizzolato, A. Sharma, K. Maute, A. Sciacovelli, V. Verda, Design of effective fins for fast PCM melting and solidification in shell-and-tube latent heat thermal energy storage through topology optimization, Appl. Energy 208 (2017) 210–227.
[17] T. Pirasaci, D.Y. Goswami, Influence of design on performance of a latent heat storage system for a direct steam generation power plant, Appl. Energy 162 (2016) 644–652.
[18] S. Seddegh, X. Wang, M.M. Joybari, F. Haghighat, Investigation of the effect of geometric and operating parameters on thermal behavior of vertical shell-and-tube latent heat energy storage systems, Energy 137 (2017) 69–82.
[19] W. Lin, Q. Wang, X. Fang, X. Gao, Z. Zhang, Experimental and numerical investigation on the novel latent heat exchanger with paraffin/expanded graphite composite, Appl. Therm. Eng. 144 (2018) 836–844.
[20] Z. Zhang, X. Fang, Study on paraffin/expanded graphite composite phase change thermal energy storage material, Energy Convers. Manage. 47 (3) (2006) 303–310.
[21] Z. Zhang, N. Zhang, J. Peng, X. Fang, X. Gao, Y. Fang, Preparation and thermal energy storage properties of paraffin/expanded graphite composite phase change material, Appl. Energy 91 (1) (2012) 426–431.
[22] V. Palomba, V. Brancato, A. Frazzica, Experimental investigation of a latent heat storage for solar cooling applications, Appl. Energy 199 (2017) 347–358.
[23] E.N. Sieder, G.E. Tate, Heat transfer and pressure drop of liquids in tubes, Indengchemres 28 (12) (1936) 1429–1435.
[24] S. Qian, Heat Exchanger Design Manual Chemical Industry Press, 2002.
[25] D.Q. Kern, Process Heat Transfer, McGRAW-Hill International Book Company, 1965.
[26] Z. He, X. Fang, Z. Zhang, X. Gao, Numerical investigation on performance comparison of non-Newtonian fluid flow in vertical heat exchangers combined helical baffle with elliptic and circular tubes, Appl. Therm. Eng. 100 (2016) 84–97.
[27] A. El Maakoul, A. Laknizi, S. Saadeddine, M. El Metoui, A. Zaite, M. Meziane, et al., Numerical comparison of shell-side performance for shell and tube heat exchangers with trefoil-hole, helical and segmental baffles, Appl. Therm. Eng. 109 (2016) 175–185.
[28] Z. Ling, J. Chen, X. Fang, Z. Zhang, T. Xu, X. Gao, et al., Experimental and numerical investigation of the application of phase change materials in a simulative power batteries thermal management system, Appl. Energy 121 (2014) 104–113.
[29] Z. Ling, J. Chen, T. Xu, X. Fang, X. Gao, Z. Zhang, Thermal conductivity of an organic phase change material/expanded graphite composite across the phase change temperature range and a novel thermal conductivity model, Energy Convers. Manage. 102 (2015) 202–208.
[30] J. Liu, Q. Wang, Z. Ling, X. Fang, Z. Zhang, A novel process for preparing molten salt/expanded graphite composite phase change blocks with good uniformity and small volume expansion, Sol Energy Mater Sol Cells 169 (2017) 280–286.
[31] Y.-T. Wu, S.-W. Liu, Y.-X. Xiong, C.-F. Ma, Y.-L. Ding, Experimental study on the heat transfer characteristics of a low melting point salt in a parabolic trough solar collector system, Appl. Therm. Eng. 89 (2015) 748–754.